Asymmetrical Functional Deficits of ON and OFF Retinal Processing in the *mdx*^{3Cv} Mouse Model of Duchenne Muscular Dystrophy

Tina I. Tsai,[1,2] Mirella Telles Salgueiro Barboni,[3,4] Balázs Vince Nagy,[3–5] Michel J. Roux,[6] Alvaro Rendon,[7] Dora Fix Ventura,[3,4] and Jan Kremers[1,8,9]

[1]Department of Ophthalmology, University Hospital Erlangen, Erlangen, Germany
[2]Department of Biology, Animal Physiology, FAU Erlangen-Nürnberg, Erlangen, Germany
[3]Núcleo de Neurociências e Comportamento, Universidade de São Paulo, São Paulo, Brazil
[4]Departmento de Psicologia Experimental, Instituto de Psicologia, Universidade de São Paulo, São Paulo, Brazil
[5]Department of Mechatronics, Optics and Engineering Informatics, Budapest University of Technology and Economics, Budapest, Hungary
[6]Translational Medicine and Neurogenetics, Institut de Génétique et de Biologie Moléculaire et Cellulaire, CNRS UMR 7104, INSERM U 964, Université de Strasbourg, Strasbourg, France
[7]Institut de la Vision/INSERM/UPMC, Univ Paris 06/CNRS/CHNO des Quinze-Vingts, Paris, France
[8]School of Optometry and Vision Science, University of Bradford, Bradford, United Kingdom
[9]Department of Anatomy II, University of Erlangen-Nürnberg, Erlangen, Germany

Correspondence: Tina I. Tsai, Department of Ophthalmology, University Hospital Erlangen, Schwabachanlage 6, 91054 Erlangen, Bavaria, Germany; Tina.Tsai@uk-erlangen.de.
Jan Kremers, Department of Ophthalmology, University Hospital Erlangen, Schwabachanlage 6, 91054 Erlangen, Bavaria, Germany; Jan.Kremers@uk-erlangen.de.

Submitted: February 25, 2016
Accepted: August 26, 2016

Citation: Tsai TI, Barboni MTS, Nagy BV, et al. Asymmetrical functional deficits of ON and OFF retinal processing in the *mdx*^{3Cv} mouse model of Duchenne muscular dystrophy. *Invest Ophthalmol Vis Sci*. 2016;57:5788–5798. DOI:10.1167/iovs.16-19432

Purpose. The dystrophin mouse mutant *mdx*^{3Cv} exhibits scotopic electroretinograpic (ERG) abnormalities, which resemble clinical changes observed in Duchenne muscular dystrophy (DMD) patients. In the present study, ERGs obtained from *mdx*^{3Cv} and their wild-type littermates under scotopic, mesopic, and photopic conditions were analyzed to provide further insight on the affected retinal pathways, and to compare them with human data.

Methods. Electroretinograms of *mdx*^{3Cv} ($n = 9$) and age-matched C57BL/6J mice ($n = 10$) included the scotopic full-field flash (for outer retinal deficits in rod pathway), scotopic threshold response (for inner retinal integrity), photopic flash, sinusoidal flicker (for outer retinal deficits in cone pathway), mesopic rapid-on/-off sawtooth flicker, and photopic long-duration flash measurements (for separate ON-/OFF-responses under different conditions).

Results. The *mdx*^{3Cv} mice exhibited diminished and delayed scotopic and photopic ERGs, particularly in their b-wave and oscillatory potentials. Interestingly, homologues to the a- and b-wave of the mesopic ON-response were affected in their peak/trough times but not in their amplitude, whereas changes to both features were uncovered for photopic ON-response and sinusoidal flicker. Mesopic and photopic OFF-components were within the norm.

Conclusions. Abnormal scotopic and photopic flash ERGs were observed in *mdx*^{3Cv}, which corroborate with deficits that are likely restricted to the level of photoreceptor-to-bipolar cell transmission. Further overlaps between *mdx*^{3Cv} mice and DMD patients exist, including asymmetrical ON versus OFF ERG alterations under mesopic versus photopic vision. In mice, ON-pathway function is compromised, whereas the OFF-pathway is spared.

Keywords: Duchenne muscular dystrophy, dystrophin, electrophysiology, mouse model

Dystrophin is a 427-kDa protein (Dp427), in which nonsense mutations in its gene (*dmd*) can cause Duchenne muscular dystrophy (DMD), a lethal, X-linked recessive muscle degenerative disease that primarily affects male children.[1] Shorter gene products of the protein, also transcribed by *dmd*, are present in different tissues.[2] The retina, for example, is a tissue where extensive expressions of the dystrophin proteins occur. Besides Dp260, the predominant retinal gene products of dystrophin found in the outer plexiform layer (OPL),[3] the full protein Dp427, and shorter DMD gene products Dp140 and Dp71 are also found at various locations in the retina (reviewed in Ref. 4).

Mouse strains lacking single or multiple dystrophin gene products have provided different models to study the mechanisms underlying electroretinographic (ERG) abnormalities in DMD patients.[5] Varying degrees of retinal dysfunction are associated with different *dmd* mutations.[6] Dp71, for example, is found around retinal blood vessels, at astrocyte perivascular processes, and at Müller cell endfeet in mice.[7–9] Its absence (i.e., in Dp71-null mice), however, is associated with only a mild but significant reduction in the scotopic b-wave in mice when assessed with the ERG,[10,11] probably due to functional compensation by dystrophin-related proteins (e.g., utrophin).[7,8,12,13] In contrast, the simultaneous absence of Dp71, the full-length Dp427, and smaller dystrophin gene products (i.e., Dp260 and 140) in the *Dmd*$^{mdx\text{-}3Cv}$ (a.k.a. *mdx*^{3Cv}) mouse, results in markedly smaller (≥40%) and delayed (~20-ms) scotopic ERG b-waves and oscillatory potentials (OPs).[14,15] These more severe functional manifesta-

Investigative Ophthalmology & Visual Science

tions are characteristic of ~80% of DMD patients, who exhibit *dmd* mutations in the central region or in the 3′ end of the gene.[5,16] In comparison to other *mdx* strains (*mdx*, *mdx*^{2Cv}, *mdx*^{4Cv}, and *mdx*^{5Cv}),[17] *mdx*^{3Cv} is currently the only mouse model that exhibits statistically smaller and slower scotopic b-wave and OPs comparable to the ERG phenotype of DMD patients. As such, the *mdx*^{3Cv} mouse has been touted to be an important model for understanding retinal anomalies in the human disease.

In addition to these pivotal in vivo studies by Pillers' group,[6,17] an in vitro transretinal ERG examination of the *mdx*^{3Cv} retina has since revealed a hypersensitivity of the rod ON-bipolar cell–driven b-wave to 2-amino-4-phosphonobutyrate (APB), a metabotropic glutamate receptor (mGluR6) antagonist.[18] The authors suggest that this phenomenon reflects malfunction(s) along the (rod) photoreceptor to rod bipolar cell synapse that are of the ON-type. In that respect, Green et al.[18] proposed hypothetical scenarios involving presynaptic changes (e.g., to rod photoreceptor glutamate release) and/or postsynaptic ON-bipolar cell changes (e.g., to binding mechanisms, concentration of indigenous glutamate, affinity and release rate of the postsynaptic binding site, and other modulatory proteins that respond to glutamate release) that could result in the b-wave amplitude and timing manifestations. However, since the effect of APB on photopic ERGs was not examined in these mice, it is unknown if the abnormal ON hypersensitivity is localized to the rod-mediated pathway.

Photopic ON/OFF ERG studies in patients and female carriers (i.e., long-flash ERGs,[19–21] sawtooth flicker ERGs, and psychophysical contrast sensitivity measurements[22]) give reason to suspect that the cone ON-pathway is also selectively altered. Interestingly, however, dysfunctions in both ON- and OFF-responses were revealed under mesopic conditions.[22] In the *mdx*^{3Cv} mouse, whether ON- and OFF-responses are differentially affected (e.g., Green et al.[18] examined only with an ON-pathway blocker[18]) and what role the state of adaptation plays have yet to be determined.

It is the purpose of the present study to compare scotopic, mesopic, and photopic ERGs using various stimulus modalities that allow the comparison of rod- and mixed rod/cone- versus cone-mediated responses; ON- versus OFF-mediated mechanisms; and outer versus inner retinal processing in wild-type and *mdx*^{3Cv} mice. This will provide further insights into the fundamental pathogenetic mechanisms that underlie retinal changes in DMD, as well as reveal whether further parallels exist between the *mdx*^{3Cv} mouse model and DMD in humans.

Methods

Animals

All animal experiments were performed in accordance with animal care guidelines established in the ARVO Statement for the Use of Animals in Ophthalmic and Vision Research and by the Society for Neuroscience. Ethics clearance from the local animal welfare authorities (Regierungspräsidium Mittelfranken, Ansbach, Germany) was also obtained.

Experiments were conducted on 9 male *mdx*^{3Cv} mice (short: DMD strain; age [mean ± SD]: 12.01 ± 1.20 months) and 10 male wild-type C57BL/6 (WT; age: 11.36 ± 0.32 months) control littermates (all 30–40 g). Age-matched controls were used to rule out any age-related changes, although muscle-[23] and scotopic ERG–related dystrophic phenotypes of younger mice of the same type (Pillers DA, oral communication, 2016) are still unchanged at this age. They were sourced from the Centre de Développement des Technologies Avancées (CDTA, Orléans, France) and transported to the Animal Physiology Department of the University of Erlangen-Nürnberg (Erlangen, Germany) 2 weeks early to acclimatize before undergoing measurements. Housing conditions adhered to the standard 12-hour light/dark cycle with water and mouse chow available ad libitum. Details regarding the generation of this *mdx*^{3Cv} mouse strain can be found elsewhere.[14,24]

Animals underwent overnight dark adaptation prior to testing. All further handling, preparation, and electrode placement (see below) were performed under deep red illumination to maintain retinal sensitivity. To maintain the body temperature during anesthesia, the animal was mounted on a water-heated platform.

In Vivo Electrophysiology

The procedure for conducting ERGs on mice has been described previously.[25,26] In short, mice were sedated with a single intramuscular injection of 50:10 mg/kg ketamine:xylazine (Ketavet; Pfizer [Berlin, Germany]; Rompun 2%; Bayer [Leverkusen, Germany], respectively), and a subcutaneous injection of saline solution (10 mL/kg, 0.9%) was given to protect them from dehydration while anesthetized. Pupils were fully dilated using tropicamide (Mydriaticum Stulln, 5 mg/mL; Pharma Stulln GmbH, Stulln, Germany) and phenylephrin-hydrochloride (Neosynephrin POS 5%; Ursapharm, Saarbrücken, Germany) eye drops (1 gutta [gtt] of each). Electroretinogram electrodes consisted of active contact lens electrodes (Mayo Corporation, Inazawa, Japan) positioned on the cornea with Corneregel (Dr. Mann Pharma, Berlin, Germany), with reference and ground needle electrodes inserted subcutaneously, medial to both ears and at the base of the tail.

Full-field ERGs (ffERGs) were recorded binocularly to a repertoire of stimuli for a detailed assessment of retinal function. Stimuli were delivered via a Ganzfeld Bowl (Roland Consult Q450SC, Brandenburg, Germany) containing six differently colored light-emitting diode (LED) arrays. The RetiPort system (Roland Consult) was used to control stimulation and data collection. All signals were amplified 100,000 times, band-pass filtered between 1 and 300 Hz, and digitized at a rate of 1024 (flicker) or 2048 Hz (flash). Table 1 shows the settings of the different full-field stimulus types performed on each animal. There were six protocols in total, which were given in order of increasing mean luminance to minimize adaptation time, until the animal woke from the single dose of anesthesia. On completion of the experiment, mice were killed on the same day by cervical dislocation under deep isoflurane-induced anesthesia for tissue harvest.

Briefly, in the first protocol, dim flashes of the red LED (λ_{max} = 639 nm, International Commission on Illumination [CIE] 1931 color coordinates: x = 0.70, y = 0.30) were presented to acquire the scotopic threshold response (STR) that reflects contributions of ganglion cells and other inner retinal components.[27] Here, 40 to 60 sweeps presented every 2 seconds (i.e., Table 1; interstimulus interval, ISI) were averaged online for every response, due to the lower signal-to-noise (SNR) ratio of dim threshold signals. A 2-second recovery time (RT) was allowed between each STR stimulus step. In the remaining five paradigms only the white LEDs (CIE 1931 color space: $x = 0.36$, $y = 0.40$) were used.

Second, a scotopic flash ERG protocol followed to assess rod- and mixed rod-cone–mediated function. Here, the number of repeats for a robust scotopic signal decreased with increasing flash strength (Table 1; sweeps). Similarly, both the RT and ISI were progressively lengthened in accordance with increasing flash strength[26] to allow complete recovery of the rod b-wave amplitude.

Table 1. ERG Recording Protocol

Protocol	Background or Mean Luminance, phot cd/m²	Flash Strength: scot cd.s/m² (log cd.s/m²)	Flash Strength: phot cd.s/m² (log cd.s/m²)	RT*, s	ISI†, s	Temporal Frequency, Hz	Sweeps
Scotopic							
(1) STR	Dark	8×10^{-6} (−5.10)‡	2×10^{-4} (−3.70)	2	2		40–60
		2.5×10^{-5} (−4.60)‡	6.3×10^{-4} (−3.20)				
		8×10^{-5} (−4.10)‡	0.002 (−2.70)				
(2) Short-flash		3.7×10^{-4} (−3.43)	2×10^{-4} (−3.70)	10	1		12
		3.7×10^{-3} (−2.43)	0.002 (−2.70)	30	2		10
		0.037 (−1.43)	0.02 (−1.70)	30	5		8
		0.37 (−0.43)	0.2 (−0.70)	60	10		8
		3.7 (0.57)	2 (0.30)	120	20		4
Mesopic (3)							
Rapid-ON sawteeth Rapid-OFF sawteeth	1			2		4	20–40
Photopic							
(4) Short-flash	25	3.70 (0.57)	2 (0.30)	2	1		20
(5) Sinusoidal flicker	60			2		3 4 6 8 12 14 18 22 26 30	20–40
(6) Long-flash, 200 ms	60	185 (2.27)	100 (2.00)		2		10

* RT, the interval allowed for rod recovery after each stimulus condition before the commencement of the next, brighter step.
† ISI, the time between repeated flashes (i.e., flash sweeps) for a given stimulus condition for short- and long-duration flash ERG protocols.
‡ Red scot cd.s/m², all others for white.

The third protocol involved luminance modulation with sawtooth temporal profiles at 4 Hz: "rapid-on" for incremental (ON-) and "rapid-off" for decremental (OFF-) responses[22,28] under mesopic conditions (preadapted to 1 phot cd/m² mean luminance for 5 minutes, 100% temporal luminance contrast). This allowed us to obtain separate ON- and OFF-driven responses, as the total response times were prolonged relative to photopic conditions (see protocol 6[29–32]). Averages of 20 to 40 episodes of 1 second each were obtained. Moreover, signals from the first two stimulus cycles (i.e., 2 seconds after stimulus onset) were discarded to avoid onset artifacts.

The fourth protocol examined cone-dominant function with the photopic flash ERG (preadapted to 25 cd/m² light background for 5 minutes). Here, 20 flashes were given every second for an average.

In protocol 5, flicker ERGs were measured to sinusoidal luminance modulation around the mean luminance of 60 phot cd/m² at 10 different temporal frequencies (3–30 Hz, 100% contrast, presented in a randomized fashion). Averages of 20 to 40 episodes were obtained, each lasting 1 second. As with the sawtooth stimuli, the first two episodes were discarded.

Finally, sixth, a 200-ms long-duration flash of 100 cd.s/m² was presented under photopic conditions to obtain a reflection of cone-driven ON- and OFF-activity. Under the photopic condition, a flash was sufficient to obtain separate ON- and OFF-responses within the limited time that was available to complete all measurements. The time after flash offset till the next repeat was 1.8 seconds.

Signal Analysis

Electroretinogram components were extrapolated offline by peak/trough detection before and/or after digital filtering in custom-written Matlab (1994–2010; The Mathworks, Inc., Ismaning, Germany) routines and Excel spreadsheets (Microsoft Office 2010; Microsoft Corporation, Redmond, WA, USA). Details regarding the extraction and analysis of major components have been published previously: flash ERGs,[2] flash OPs,[33] sawtooth flicker ERG,[34] sinusoidal flicker ERG.[35]

Briefly, (1) the STR was defined as the positive (pSTR) peak to negative (nSTR) trough (at approximately 120 and 220 ms after stimulus onset, respectively). (2) In the scotopic flash ERG, the a-wave was defined as the difference between baseline and the minimum within 50 ms post stimulus onset, and the b-wave was the difference between the a-wave minimum and the b-wave maximum after digital removal of OPs in the Fourier frequency domain from the leading ascending limb with a square, 50- to 300-Hz band-pass filter. Isolated OPs (i.e., filtered signals after inverse Fourier transform back to the time domain) were measured as trough to peak of wavelets OP_2 to OP_4, with OP_3 being of the largest amplitude. The peak and trough times of each of the aforementioned components were also calculated from onset of the stimulus. A 30- and 16-ms prestimulus epoch was recorded for the STR and scotopic flash ERGs, respectively, which allowed for offline baseline measurement.

(3) For sawtooth ERGs, baseline was defined as the average of the first 5 ms of each response after the rapid luminance change. The first troughs (i.e., N1 of the ON- and OFF-

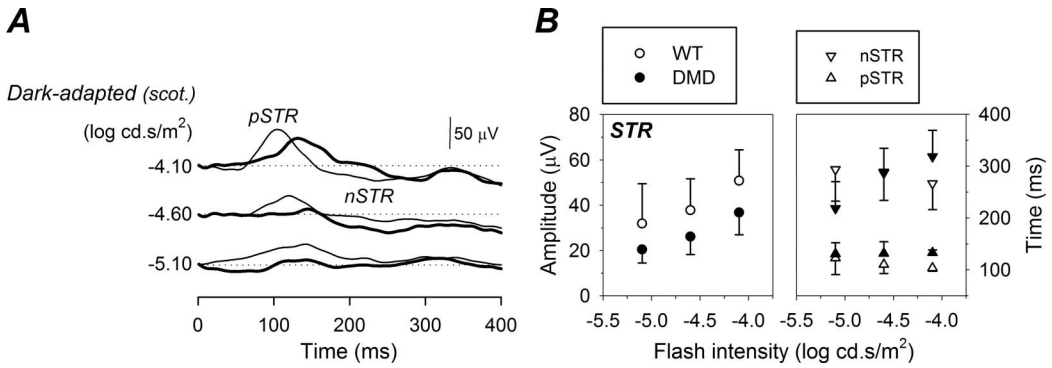

Figure 1. Comparison of the DMD mutation on the STR. (**A**) Average DMD (*bold traces*, $n = 8$) and WT (*thin traces*, $n = 8$) waveforms elicited by red, dim threshold LED flashes (shown *left* of traces; see Table 1 for conversion to other units) under dark-adapted conditions. The nomenclature of key components analyzed (pSTR, nSTR) that make up the STR, and zero reference (*horizontal dotted*) lines are provided. (**B**) Grouped parameter amplitude (µV, *left*, mean ± SD) and peak/trough time values (ms, *right*) of key components are given as a function of flash intensity (log scot cd.s/m^2) for WT (*unfilled symbols*) and DMD mice (*filled symbols*).

responses; N_{ON} and N_{OFF}) were taken from baseline, with subsequent component amplitudes (P_{ON}, LN_{ON}, P_{OFF}) calculated as "peak to peak" from the preceding peak trough. The sawtooth waveforms were additionally low pass filtered at 40 Hz to remove mains noise before the extraction of parameters. This is the first study, to our knowledge, to record sawtooth flicker ERG in the mouse; thus the nomenclature defined for the human response[34] was adopted. A feature in the human rapid-off sawtooth response that is not apparent in the mouse sawtooth ERG, however, is the presence of an initial positivity homologue to the d-wave.[36] Possibly, the P_{OFF} is a homologue of a late component because it has a similar peak/trough time as the LN_{ON} (see Results). However, this component is a positive deflection. Thus, mesopic measures of the inner retinal integrity were possibly achieved in this study by measuring the LN_{ON} and the P_{OFF} All peak/trough times were defined as the time between stimulus onset and the minimum/maximum components.

(4) In the photopic short-flash ERG, only the b-wave was considered, as both the photopic a-wave and the photopic negative response (PhNR) were insignificant (<5 µV).[37,38] As with the scotopic ERG, there was also a 16-ms prestimulus epoch for establishing baseline.

(5) Steady-state flicker ERGs underwent Fourier analysis to isolate the first harmonic component and phase. Noise level was defined as the mean amplitude at frequencies ± 1 Hz of the stimulus frequency. This was subtracted from each raw amplitude to provide the final noise-corrected values. The first harmonic amplitudes and timing values were accepted for analysis only if the SNR was larger than two. Although timing values of such "close to zero" amplitudes are indeed noninformative, we acknowledge that discarding the very small amplitudes themselves may introduce a bias toward large amplitudes. This, however, was probably negligible as it occurred for the same number of WT and DMD 3- and 4-Hz datasets.

(6) In the photopic long-flash signal, a robust a-wave is evident (in comparison to the short-flash signal in this study), which allowed cone photoreceptor and OFF-bipolar cell integrity to be assessed.[39] Following this component is the P_{ON} (probably homologue to the b-wave), which reflects the ON-response. As in the measurements with the mesopic sawtooth stimuli, we confirm previous observations that stimulus offsets do not elicit a d-wave in the mouse.[36] Instead, the OFF-response was measured as the negative deflection (called N_{OFF}) approximately 150 ms after stimulus offset, measured from the second baseline (after stimulus offset). The peak time of the a-wave and P_{ON} was measured from stimulus onset, whereas N_{OFF} was measured from the offset of the stimulus.

Data representation graphics were generated with Sigmaplot (v12.3; Systat Software, Inc., Erkrath, Germany) and Matlab.

Statistics

Comparisons of DMD and WT components were carried out in Excel (Microsoft Office 2010) and Prism (Prism v5.00; GraphPad Software, Inc., San Diego, CA, USA). Since all experimental data exhibited Gaussian distributions (Komogorov-Smirnov normality test, $P < 0.01$, Prism), parametric statistics such as Student's *t*-test (2-tailed, unpaired) were employed to test the significance of differences between single WT and DMD parameters (i.e., photopic flash ERG and sawtooth flicker ERG). Two-way repeated measures (RM)-ANOVA (ERG versus strain and intensity) were adopted to evaluate datasets across a series of flash strengths (for scotopic flash ERG and STR measurements) or temporal frequencies (sinusoidal flicker ERG). The α value was 0.05, except for multiple comparisons, where it was adjusted to 0.01 to protect against Type I errors. When ANOVA revealed a significant interaction between strain and intensity or temporal frequency, Bonferroni post hoc tests were used to evaluate amplitude and/or phase differences among individual intensities or frequencies.

Additionally, response phases as a function of temporal frequency were modeled with a linear regression ($y = y_0 + ax$), as described by Kremers and Scholl.[40] The parameter a, which describes the slope (i.e., a measure of phase change with frequency in °/Hz), then allowed the phase relationships between the two mouse strains to be compared with 1-way ANOVA (Prism; i.e., set up with mean = a, SEM = SD of a, N = dF+1). This is equivalent to conducting an analysis of covariance (ANCOVA) for comparing linear regressions.

Results

Scotopic Threshold Responses

Figure 1A displays STR-like waveforms elicited with red flashes dimmer than –4.10 log scot cd.s/m^2 after averaging the responses obtained from all animals. They were made up of a pSTR followed by a slower nSTR for WT mice (Fig. 1A, thin traces). Comparisons with STRs recorded from DMD mice (Fig. 1A, bold traces) indicate somewhat smaller and slower

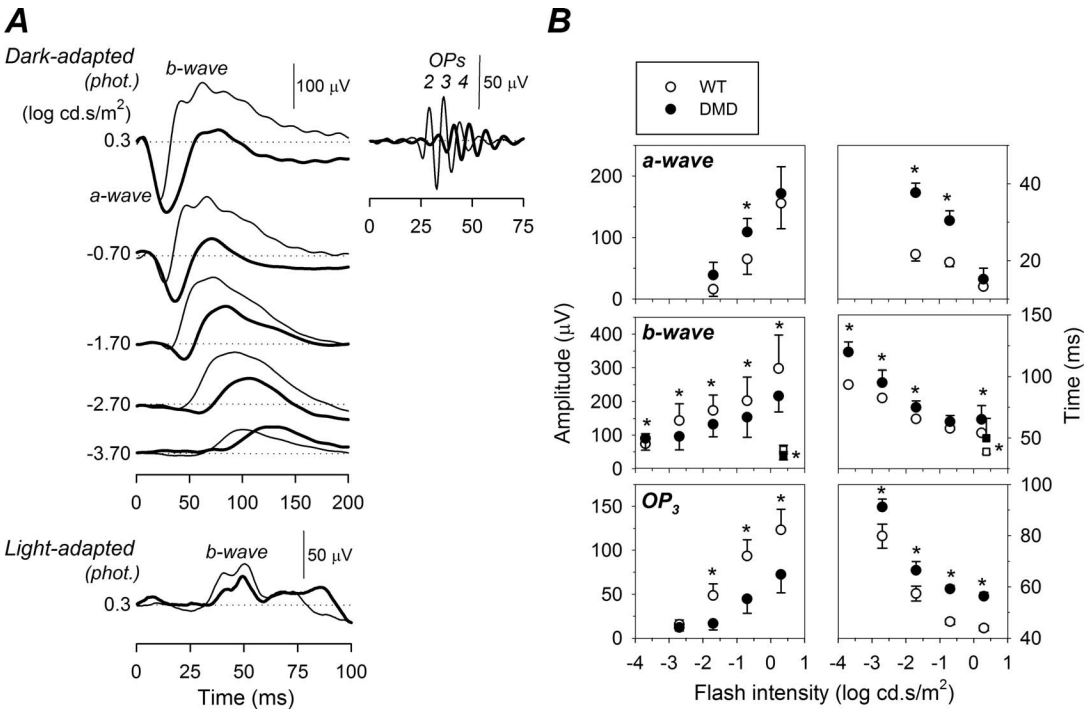

FIGURE 2. Comparison of scotopic and photopic flash ERG waveforms between DMD and WT mice. (**A**) Average DMD (*bold traces*, $n = 5$–9) and WT (*thin traces*, $n = 5$–10) waveforms elicited by intermediate to moderately bright white scotopic (*top*) and a single photopic flash (*bottom*). Flash intensities are shown to the *left* of traces, and nomenclature of key components analyzed (a-wave, b-wave, isolated scotopic OPs 2–4) is provided. Representative OPs isolated from the top flash strength (0.3 log cd.s/m^2) are shown to the *right* of the corresponding scotopic ERG. Zero references (*horizontal dotted*) lines are provided for select responses to aid comparisons. (**B**) Grouped parameter amplitude (µV, *left*, mean ± SD) and peak/trough time values (ms, *right*) of key components are given as a function of flash strength (log phot cd.s/m^2) for WT (*unfilled symbols*) and DMD mice (*filled symbols*). Photopic b-wave (*square symbols*) amplitude and peak time plots are overlaid in the scotopic b-wave image (*circular symbols*, offset *right* and *left* of 0.3 log cd.s/m^2, respectively), and only OP_3 is plotted as a representative of OP changes. See Figure 3D for photopic a-wave comparisons. Note that parameters are shown only at relevant intensities, and those that are significantly different between WT and DMD groups are marked with an *asterisk*.

waveforms. However, when their respective parameters (mean ± SD; DMD, filled symbols versus WT, unfilled symbols) were plotted as a function of stimulus intensity (Fig. 1B), parameter differences between DMD and WT animals did not reach significance (amplitude: approximately −32%, 2-way RM-ANOVA; $P = 0.84$, peak/trough times: pSTR +28 and nSTR +50 ms at −4.10 log scot cd.s/m^2, both $P = 0.02$).

Flash ERGs

Figure 2A shows averaged dark- (top) and light-adapted flash ERG responses (bottom) from WT (thin traces) and DMD (bold traces) mice. Responses from both groups grew with increasing scotopic flash intensity. White light flashes of −3.70 log phot cd.s/m^2 and brighter elicited conventional rod-driven ERGs. The positive potential, known as the ON-bipolar cell–mediated b-wave, dominated (with time to peak decreasing from ∼100 to 70 ms with increasing intensities) until high-frequency OPs on its ascending limb (between 44 and 80 ms) and a preceding a-wave negativity intruded from −1.70 log phot cd.s/m^2 (22–13 ms). The a-wave and OPs allow the assessment of photoreceptoral and inner retinal feedback functions, respectively.[33,41] Under light-adapted conditions, a photopic ERG mainly composed of a positive b-wave (at approximately 40 ms) was elicited to a moderate 2 phot cd.s/m^2 flash.[38,39,42] Other photopic components of the short-flash ERG were not considered at this setting (see Methods). Analysis of the photopic a-wave in this section was assessed from the photopic long-flash ERG (Figs. 3C, 3D) rather than the short-flash response (Figs. 2A, 2B) because the brighter long flash used (100 vs. 0.3 cd/m^2 here) evoked a larger a-wave component. This allowed the contributions from both cone photoreceptors and OFF-bipolar cells to be examined.[39]

Inspection of DMD waveforms (bold traces) superimposed on those of WT (thin traces) showed that the scotopic OPs, scotopic b-wave, and, minimally, the photopic b-wave may exhibit reduced amplitudes. Particularly in the scotopic signals, larger a-wave components were revealed with the reduction of the b-waves. The initial a-wave slopes appear, however, unchanged, reflecting the likelihood of normal phototransduction. Timing alterations were also evident in DMD responses elicited under scotopic conditions.

Figure 2B demonstrates the relationship between stimulus intensity and WT (unfilled symbols) and DMD (filled symbols, mean ± SD) ERG amplitude (left) and timing (right). Parameter comparisons revealed an appreciably larger and prolonged scotopic a-wave in DMD mice (circular symbols in upper plots; approximately +37% and +16 ms, both $P < 0.01$). The change in both a-wave features was, however, significant only at −0.70 log phot cd.s/m^2, and not to brighter or dimmer flashes. A similarly supernormal and later a-wave was also noted in the photopic (long-flash) ERG response (+40% and +9 ms; Figs. 3C, 3D); however, given its much smaller SNR, only the timing change reached significance (photopic a-wave amplitude Δ: *t*-test $P = 0.09$, and trough time Δ: $P = 0.03$).

Significantly smaller and slower (to peak) scotopic b-waves (up to −33% and +25 ms relative to WT; middle left plot), OPs (OP_2: −27%, OP_3: −41%, OP_4: −39%, and OP_3 by up to

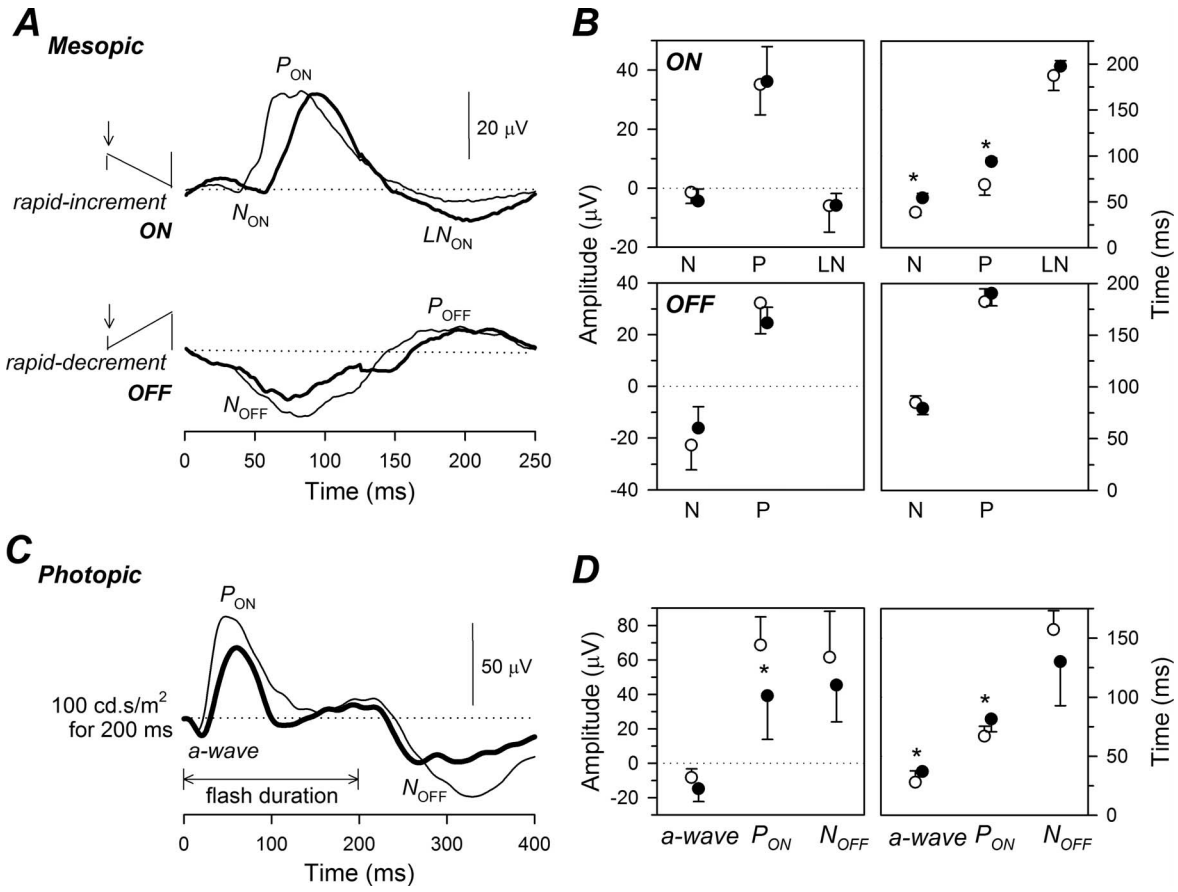

Figure 3. Comparison of ON- and OFF-mediated ERG components. (**A**) Mesopic ON-/OFF-components are elicited independently by periodic sawtooth stimuli. Shown are 250-ms epochs of average DMD (*bold*, $n = 7$) and WT mice (*thin*, $n = 10$) traces to one period of stimulation. In comparison, (**C**) photopic ON- and OFF-components were elicited consecutively to a bright (100 cd.s/m^2), long (200-ms) flash (DMD, *bold trace*, $n = 9$; WT, *thin trace*, $n = 6$). Key nomenclature includes N_{ON}, P_{ON} , and LN_{ON} for mesopic ON; N_{OFF} and P_{OFF} for mesopic OFF; and a-wave, P_{ON}, and N_{OFF} for photopic ON and OFF ERGs. Zero reference (*horizontal dotted*) lines are provided to aid comparisons. Average (±SD) amplitude (*left*) and peak/trough time parameters (*right*) of mesopic and photopic ON/OFF ERGs from WT (*unfilled symbols*) and DMD mice (*filled symbols*) are shown in (**B**, **D**), respectively. Components that are significantly different between WT and DMD groups are marked with an *asterisk*.

approximately +13 ms; lower left plot only data for OP_3 are displayed), and the photopic b-wave (square symbols in the middle left plot, approximately −28% and +11 ms), on the other hand, were confirmed across the full intensity range measured in the DMD group (scotopic: 2-way RM-ANOVAs $P < 0.01$; photopic: $P \geq 0.02$). Of note is that the peak/trough time changes in both scotopic a- and b-waves generally decreased with increasing flash intensity.

ON-OFF ERGs

In Figure 3A, the averaged ERGs to periodic sawtooth flicker stimulation are shown, which evoked separate onset (ON-) and offset (OFF-) responses. The mouse mesopic ON-response presented here is similar to the human response.[22,43] It is composed of a very small first negative trough (N_{ON}), a positive peak (P_{ON} ~69 ms post onset), and a late negativity (LN_{ON} ~187 ms). The mesopic OFF-response in comparison has an initial slow negativity that reaches a maximum of approximately 85 ms after stimulus onset (N_{OFF}). This is followed by a peak (P_{OFF}) that is slower and later than the photopic (~182 ms). Moreover, mouse mesopic ON- and OFF-responses appear to be mirror images of one another in terms of peak/trough times ($P_{ON} \approx N_{OFF}$ and $LN_{ON} \approx P_{OFF}$). As mentioned above, the mirror imaged components may have similar cellular origins.

Some differences between WT (thin traces) and DMD mesopic ON-/OFF-responses (bold traces) are evident. Group data shown in Figure 3B indicate that both N_{ON} and P_{ON} amplitudes (left) are similar in size in DMD and WT mice ($P = 0.15$ and 0.86, respectively), but reach their respective maxima approximately 16 and 25 ms later in DMD mice (filled symbols; both $P < 0.01$, Fig. 3B; right). In contrast, LN_{ON} of the mesopic ERGs were similar in amplitude and time ($P = 0.97$ and 0.13, respectively). Likewise, differences between DMD and WT mesopic N_{OFF} and P_{OFF} responses did not reach significance (amplitude: $P = 0.14$ and 0.12, peak/trough time: $P = 0.09$ and 0.18, respectively).

At photopic luminance levels, Figure 3C presents an a-wave (discussed above in the Flash ERGs section), followed by an ON- (P_{ON}) and subsequent OFF-components (N_{OFF}) evoked from a bright, long-duration flash. Here, ON-/OFF-responses are not completely dissociated as for corresponding mesopic signals (Fig. 3A), but are consecutively evoked components on the one waveform. Furthermore, the flash time was long enough to separate ON- and OFF-responses. Parameter summaries (Fig. 3D) reveal that the photopic P_{ON} is significantly smaller (approximately −41%, $P = 0.04$) and slower (approximately +14 ms, $P = 0.02$) in DMD. In contrast, relatively smaller differences in photopic N_{OFF} between the two groups did not reach significance (amplitude approximately −26%: $P = 0.21$, trough time approximately −27 ms: $P =$

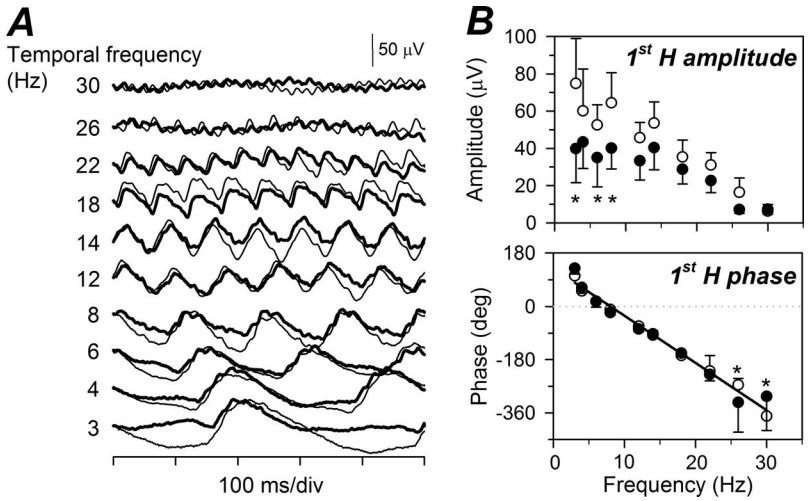

Figure 4. Comparison of flicker ERGs. Average ERG (**A**) waveforms from DMD (*bold traces*, $n = 9$) and WT mice (*thin traces*, $n = 10$). Traces show the first 500-ms sections of the 1-second flicker response. Temporal frequencies of the flicker stimuli used to elicit these signals (*left side* of traces) were presented with mean luminance of 60 cd/m^2 at 100% contrast. (**B**) Comparison of flicker ERG amplitude (*top*, µV) and phase (*bottom*, degrees) parameters (mean ± SD) is presented as a function of stimulus frequency. DMD, *filled symbols*; WT, *unfilled symbols*; significant difference between WT and DMD, *asterisk*.

0.12). Taken together, the temporal course of both the mesopic and photopic ON-response is slower in DMD mice, whereas its amplitude is additionally reduced under the photopic condition. OFF-responses, on the other hand, remain largely unchanged regardless of mean luminance.

Sinusoidal Flicker ERGs

When flicker stimuli were used to examine the integrity of postreceptoral processing, DMD waveforms (Fig. 4A, bold traces) showed similar trends as WT responses (thin traces) in response to our repertoire of temporal frequencies (3–30 Hz, bottom to top, indicated at left). At first glance, flicker responses from DMD mice appear smaller in size than those of WT, with no apparent shift in phase across the frequency range. Smaller fundamental amplitudes of DMD signals (filled symbols) in comparison to WT signals (unfilled symbols) were confirmed (approximately –45%, 2-way RM-ANOVA $P < 0.01$) in Figure 4B frequency–response profiles (top). In fact, post hoc analysis revealed that responses to sinusoidal flickers of lower temporal frequencies were particularly affected in DMD mice (strain*frequency, $P < 0.01$ for 3, 6, and 8 Hz). Despite this, phase behaviors of the two groups exhibited comparable linear frequency–phase relationships ($P = 0.74$, both $r^2 > 0.96$) except at 26 and 30 Hz (strain*frequency, $P = 0.01$). Both relationships had slopes of approximately 16°/Hz corresponding to apparent latencies of approximately 44 ms ($P = 0.98$).

Discussion

We employed an extensive ERG repertoire to further the functional evaluation of retinal health in the *mdx*^{3Cv} mouse. Currently, this genotype is still considered the most representative animal model of the retinal changes in DMD patients with mutations downstream of exon 30.[6] In addition to the characteristic smaller and slower b-wave to a bright, white, scotopic flash indicating rod ON-bipolar cell–related dysfunction, an ERG phenotype not pathognomonic for DMD,[19,44] we recognize that mechanisms associated with cone ON-bipolar cell neurotransmission are also affected in the *mdx*^{3Cv} mouse . This sits well with the fact that both cone-dominant Dp427 and rod-dominant Dp260 are affected in the *mdx*^{3Cv} mice.[4] However, because the standard flash b-wave also contains some contributions from the OFF-subnetwork, separate ON- and OFF-only activity were additionally assessed. Here we attempt to tie together the similarities and differences in ERG features from the current DMD model and humans (summarized in Table 2). We would like to point out that the changes reported below are due to the genetic differences between the different mouse groups (i.e., are a part of the DMD disease), as age-matched WT mice were used to control for any age-related influences.

Rod-Mediated Function in *mdx*^{3Cv}

As mentioned above, the scotopic short-flash ERG has been recorded routinely to screen DMD patients[15,20] and mice with various deletions in the dystrophin gene.[6,18,45] In the current study, the expected reduction and delay of the rod-mediated ON-bipolar cell b-wave in the *mdx*^{3Cv} line were evident from intermediate to bright flashes of –2.70 to 0.30 log phot cd.s/m^2 (Fig. 2). It may be noted that our maximum scotopic b-wave does not appear as "electronegative" as that reported in Pillers' study[6,17] (e.g., up to –33% vs. –59%), probably due to the brighter flash used in their study (i.e., data presented for 0.8 vs. 0.3 log cd.s/m^2 used here). However, the same qualitative change is seen in the scotopic b-wave amplitude, and the peak time was prolonged to the same degree (~25 ms).

Similarly, scotopic OPs were attenuated (approximately –41%) and delayed (+13 ms) in the *mdx*^{3Cv} group, as in previous recordings from mice of this genotype. These changes have also been consistently seen in DMD patients [16,46] (Table 2). The recent discovery of additional Dp427 mRNA closer to the inner nuclear layer in mice (likely in OFF-bipolar and amacrine cells[4]) may indicate its involvement in amacrine–OFF-bipolar cell feedback interactions, touted to be the likely generators of the OPs.[47–50] Normal OPs in Dp71-null,[10] *mdx*^{5Cv}, and *mdx* mice (in which Dp427 is selectively knocked out[6]), but not in strains additionally deficient for Dp260 (*mdx*$^{2Cv\text{-}4}$), suggest that both Dp427 and Dp260 are involved in the generation of these oscillations (similar to the suggested importance of both Dp260 and Dp71, rather than either one alone, for a normal scotopic b-wave[6,11]).

Table 2. Tabulated Overview of ERG Results From *mdx*^{3Cv} Mice in the Current Study Compared to Published Results on DMD Patients

ERG	Retinal Component	*mdx*^{3Cv} Mouse	DMD Patient
STR	Inner retinal activity	Secondary effect on STR amplitude and timing from upstream b-wave changes	N/A
Scotopic short flash	Rod-driven pathway	Markedly smaller and slower b-wave Markedly smaller and slower OPs Supernormal and slower a-wave Smaller b/a amplitude ratio	Electronegative and slower b-wave[15,16,19,20,46] Markedly smaller and/or missing OPs[15,16,20,46] Supernormal[16,17,54] or unaffected a-wave[46] Smaller b/a amplitude ratio[16,17]
Photopic short flash	Cone-driven pathway	Smaller and slower b-wave (OPs not analyzed)	Mildly smaller or nearly normal b-wave, with missing OP_2[5,16,19,20,46,61]
Mesopic sawtooth	Mixed rod/cone-driven ON/OFF processing	Delayed N_{ON} and P_{ON} with normal amplitudes OFF-response within the norm	Smaller positive peaks of ON- and OFF-response amplitudes with no timing change[22]
Photopic sawtooth	Cone-driven ON/OFF processing	N/A	Smaller positive peaks of ON-response amplitude with no timing change[22] OFF-response within the norm[22]
Photopic long flash		Smaller and slower ON-component OFF-component within the norm	Smaller and slower ON-component OFF-component within the norm[19,20]
Photopic sinusoidal flicker	Cone-driven postreceptoral processing	Smaller amplitudes to 6- to 8-Hz flickers, with no phase change	Normal amplitudes to 30-Hz flicker, but a more sawtooth-like profile[15,20,46]

N/A, not applicable.

As a result of the subnormal and slower appearance of the scotopic b-wave–OP complex, the preceding rod a-wave appeared supernormal and delayed. This feature has been noted in both *mdx*^{3Cv} mice and DMD patients alike[6,16,18] (Table 2). As previously explained by Pillers et al.,[6] it likely is a secondary effect from lesser and delayed opposing b-wave revealing the underlying "slow PIII,"[51–53] given identical a-wave slopes (hence, kinetics[41]). Not surprisingly, b/a amplitude ratios here were thus significantly smaller (1.3 vs. 2.5 in WT; as seen in humans and mice[17,54]).

What to date has not been examined in the *mdx*^{3Cv} strain is the functional integrity of inner retinal neurons, in particular, the retinal ganglion cells (RGCs). Based on previous observations in rat ffERGs[55] a reduced input from upstream elements (e.g., from photoreceptors or bipolar cells) should by default result in at least the same proportion of reduced downstream output (e.g., to bipolar or ganglion cells). As such, a secondary effect of the DMD-induced b-wave reduction on the STR response was anticipated. Indeed, STRs of *mdx*^{3Cv} mice were found to be reduced and delayed by a similar magnitude as the scotopic b-wave (approximately −32%, +28 ms). However, these changes lacked significance (Fig. 1), possibly due to the smaller SNR of the dim threshold response. Still, the non-significance of the STR changes also suggests that the mislocalization (but normal membrane expression) of K^+ channels in Müller cell endfeet as a result of altered Dp71 expression in *mdx*^{3Cv} [7,11,56] may not have extinguished or sufficiently impaired Müller cell control of retinal K^+ homeostasis.[57] Otherwise, the STR would be halved, as seen in mice lacking the principal inward rectifying Kir4.1 channels that underlie K^+ buffering.[58] Clinically normal pattern-reversal visual evoked potentials (an indirect indicator of intact optic nerve and RGC function[59]) in DMD patients[46,60] are also consistent with the notion that RGC activity is not directly affected in the disease.

Cone-Mediated Function in *mdx*^{3Cv}

Here, we report for the first time, a significant loss and increased peak time of the cone-mediated b-wave in *mdx*^{3Cv} mice. In comparison to the above-mentioned rod changes, the cone-mediated a-wave (in the long-flash ERG; Figs. 3C, 3D) also appeared supernormal, suggesting that the cone photoreceptors are also spared. The cone b-wave defect, however, was somewhat milder than that of the rod b-wave (∼5% less reduced and 14 ms less delayed than rod-mediated b-waves). That both rod and cone pathways are affected is not surprising, since both Dp427 and Dp260 expression have been described in mouse rod and cone photoreceptor terminals.[4,9] Actually in the mouse, a proportionally greater amount of Dp427 was found in cone than in rod synapses. It is therefore interesting that cone-mediated function was affected to a lesser extent than rods. More studies would need to be conducted to uncover the reason behind this bias. In DMD patients, a mild reduction of the photopic b-wave has only sometimes been noted[5,16,20,46,61] (Table 2).

Our photopic sinusoidal flicker data also corroborate with a postreceptoral defect in the cone pathway (Fig. 4). They also provided novel evidence of a temporal frequency–specific effect, since signals to ≤8 Hz-modulations were more affected than those evoked by higher temporal frequencies. In mammalian retinae, distinct transient and sustained postreceptoral mechanisms are present.[62] Human ERGs to sinusoidal stimuli have been found to reflect activity of the parvocellular and magnocellular pathways[63] (if not homologue, then at least analogue to sustained and transient mechanisms in nonprimate mammals[64–66]). Assuming that the mouse ERG to sinusoidal modulation reflects similar mechanisms, the response decrease at low temporal frequencies suggests a selective effect on the sustained process. Future studies employing more advanced flicker ERG paradigms (e.g., incorporating silent substitution techniques) could be instrumental for uncovering any pathway-specific postreceptoral changes. In comparison to flashes, sinusoidal modulation paradigms also provide "cleaner" results, since responses to different stimulus settings can be assessed under identical adaptation conditions independent of stimulus strength and temporal frequency. Furthermore, the stimulus contains only one frequency component (versus flashes, which contain higher harmonics). Unlike the situation with flashed stimuli, the presence of higher harmonics in the response can thus be definitely attributed to physiological nonlinearities when sinusoidal stimuli are used.

With all this taken together, we show that *dmd* mutation in *mdx*^{3Cv} mice alters the responsiveness of second-order neurons

in both rod and cone photoreceptor pathways, namely, of the bipolar cells and modulatory amacrine cells. Any downstream consequences on RGC output are likely an indirect effect of the upstream change. Whether the Dp427-specific loss of cone signals, as recently discovered in human patients,[16] also exists in DMD mouse models requires further exploration.

ON- Versus OFF-Pathway Function in *mdx*^{3Cv}

Asymmetrical dysfunction of ERGs evoked by onset versus offset sawtooth stimuli has been noted under mesopic and photopic backgrounds in DMD patients (with gene alterations downstream of exon 30).[22] Specifically, the positive peaks of the mesopic ON- and OFF-responses were equally reduced, whereas photopic ON-responses were more diminished than the photopic OFF[19,20,22]. In our *mdx*^{3Cv} cohort, we also found ON-responses to be more affected than OFF-responses in the ERG. The difference here, however, was that an ON-pathway–specific deficit was already manifest under mesopic (in addition to photopic) conditions (Fig. 3; Table 2), and responses mediated by OFF-mechanisms of both mesopic and photopic systems were not affected. That the a-wave of the photopic long-flash ERG was not smaller in these mice provides further support for normal photoreceptor and OFF-bipolar cell functioning.[39] Furthermore, state of adaptation–dependent deficits were seen. Specifically, mesopic ON ERGs in *mdx*^{3Cv} mice exhibited only a significant temporal change (i.e., no amplitude difference), whereas photopic ON-responses were delayed in addition to being reduced. In comparison, DMD patients in the previous studies showed amplitude but not timing changes.

The differences in results between data from patients and *mdx*^{3Cv} mice may in part be due to species differences in how dystrophin maintenance of cellular functions is affected in the retina. This is not surprising since differences in the functional readout of dystrophin deficiencies between DMD patients and dystrophin-null mice (i.e., in *mdx* and *mdx*^{3Cv}) have already been noted for the signature muscle phenotype (reviewed in Refs. 67, 68). Specifically, the mice display signs of only mild muscle dystrophy and an unsubstantially shorter life span despite showing the same dystrophin deficiencies in the muscle surface membranes compared to human patients, who display severe muscle dystrophy and substantial decrease of life expectancy. A recent but yet to be proven idea is that the upregulation of functional compensatory mechanisms in cells coexpressing a dystrophin product with utrophin (i.e., a potential dystrophin surrogate) may be better in mice than in humans,[68] complicating comparisons of their symptoms. Alternatively or additionally, the aforementioned differences in sawtooth ERG results could have also arisen if the cellular contributors of human versus mouse sawtooth signals differed. The exact origins of these have yet to be established. Nevertheless, a proportionally greater photopic ON-pathway dysfunction in DMD is still inferred in both model and humans.

The interpretation of ON dysfunction reported here is also in line with in vitro data from Green and colleagues,[18] which highlighted an abnormal responsiveness of ON-bipolar cell activity. The vulnerability of the OFF transmission in the *mdx*^{3Cv} retinae has yet to be examined in the same way.

In conclusion, electrophysiological manifestations of retinal changes in the *mdx*^{3Cv} mice have been further defined. Apart from the major amplitude and timing changes to the scotopic b-wave and OPs, we also report additional alterations in mesopic and photopic ON-mechanisms, as well as other postreceptoral changes that bear resemblance to newly reported electrophysiological and psychophysical findings in DMD patients with mutations at the 3′ gene end.[22] The *mdx*^{3Cv} genotype therefore continues to be a promising model for better understanding the retinal anomalies associated with DMD in humans. Moreover, the ERG continues to provide novel information under both laboratory and clinical settings, and thus warrants further exploration in DMD research. Not only does it provide a noninvasive means to monitor DMD disease severity, but it could ultimately be used to assess the success of potential gene therapy treatments.

Acknowledgments

Supported by the German Research Foundation (DFG KR1317/13-1; JK), Federal Ministry of Education and Research of Germany (BMBF 01DN14009; JK), São Paulo Research Foundation (FAPESP 2014/06457-5, BVN; FAPESP 2007/55125-1, MTSB; FAPESP 2012/01115-3; DFV), joint Bavarian Academic Center for Latin America and São Paulo Research Foundation program (FAPESP-BAYLAT 2012/51299-3; DFV, JK), Brazilian National Council for Scientific and Technological Development (CNPq 470785/2014-4, MTSB; CNPq 490428/2013-4, DFV), and the Association Française contre les Myopathies (AFM 14853; AR).

Disclosure: **T.I. Tsai**, None; **M.T.S. Barboni**, None; **B.V. Nagy**, None; **M.J. Roux**, None; **A. Rendon**, None; **D.F. Ventura**, None; **J. Kremers**, None

References

1. Hoffman EP, Brown RH, Kunkel LM. Dystrophin: the protein product of the Duchenne muscular dystrophy locus. *Cell*. 1987;51:919–928.
2. Muntoni F, Torelli S, Ferlini A. Dystrophin and mutations: one gene, several proteins, multiple phenotypes. *Lancet Neurol*. 2003;2:731–740.
3. D'Souza VN, Nguyen TM, Morris GE, Karges W, Pillers DA, Ray PN. A novel dystrophin isoform is required for normal retinal electrophysiology. *Hum Mol Genet*. 1995;4:837–842.
4. Wersinger E, Bordais A, Schwab Y, et al. Reevaluation of dystrophin localization in the mouse retina. *Invest Ophthalmol Vis Sci*. 2011;52:7901–7908.
5. Sigesmund DA, Weleber RG, Pillers DA, et al. Characterization of the ocular phenotype of duchenne and becker muscular-dystrophy. *Ophthalmology*. 1994;101:856–865.
6. Pillers DA, Weleber RG, Green DG, et al. Effects of dystrophin isoforms on signal transduction through neural retina: genotype-phenotype analysis of Duchenne muscular dystrophy mouse mutants. *Mol Genet Metab*. 1999;66:100–110.
7. Fort PE, Sene A, Pannicke T, et al. Kir4.1 and AQP4 associate with Dp71- and utrophin-DAPs complexes in specific and defined microdomains of Muller retinal glial cell membrane. *Glia*. 2008;56:597–610.
8. Sarig R, Mezger-Lallemand V, Gitelman I, et al. Targeted inactivation of Dp71, the major non-muscle product of the DMD gene: differential activity of the Dp71 promoter during development. *Hum Mol Genet*. 1999;8:1–10.
9. Howard PL, Dally GY, Wong MH, et al. Localization of dystrophin isoform Dp71 to the inner limiting membrane of the retina suggests a unique functional contribution of Dp71 in the retina. *Hum Mol Genet*. 1998;7:1385–1391.
10. Cia D, Simonutti M, Fort PE, Doly M, Rendon A. Slight alteration of the electroretinogram in mice lacking dystrophin dp71. *Ophthalmic Res*. 2014;51:196–203.
11. Dalloz C, Sarig R, Fort P, et al. Targeted inactivation of dystrophin gene product Dp71: phenotypic impact in mouse retina. *Hum Mol Genet*. 2003;12:1543–1554.
12. Dalloz C, Claudepierre T, Rodius F, Mornet D, Sahel J, Rendon A. Differential distribution of the members of the dystrophin glycoprotein complex in mouse retina: effect of the mdx(3Cv) mutation. *Mol Cell Neurosci*. 2001;17:908–920.

13. Galvagni F, Cantini M, Oliviero S. The utrophin gene is transcriptionally up-regulated in regenerating muscle. *J Biol Chem*. 2002;277:19106–19113.
14. Cox GA, Phelps SF, Chapman VM, Chamberlain JS. New mdx mutation disrupts expression of muscle and nonmuscle isoforms of dystrophin. *Nat Genet*. 1993;4:87–93.
15. Cibis GW, Fitzgerald KM, Harris DJ, Rothberg PG, Rupani M. The effects of dystrophin gene mutations on the ERG in mice and humans. *Invest Ophthalmol Vis Sci*. 1993;34:3646–3652.
16. Ricotti V, Jagle H, Theodorou M, Moore AT, Muntoni F, Thompson DA. Ocular and neurodevelopmental features of Duchenne muscular dystrophy: a signature of dystrophin function in the central nervous system. *Eur J Hum Genet*. 2016;24:562–568.
17. Pillers DA, Weleber RG, Woodward WR, Green DG, Chapman VM, Ray PN. mdxCv3 mouse is a model for electroretinography of Duchenne/Becker muscular dystrophy. *Invest Ophthalmol Vis Sci*. 1995;36:462–466.
18. Green DG, Guo H, Pillers DA. Normal photoresponses and altered b-wave responses to APB in the mdxCv3 mouse isolated retina ERG supports role for dystrophin in synaptic transmission. *Vis Neurosci*. 2004;21:739–747.
19. Cibis GW, Fitzgerald KM. The negative ERG is not synonymous with nightblindness. *Trans Am Ophthalmol Soc*. 2001;99:171–175, discussion 175–176.
20. Fitzgerald KM, Cibis GW, Giambrone SA, Harris DJ. Retinal signal transmission in Duchenne muscular dystrophy: evidence for dysfunction in the photoreceptor/depolarizing bipolar cell pathway. *J Clin Invest*. 1994;93:2425–2430.
21. Fitzgerald KM, Cibis GW, Gettel AH, Rinaldi R, Harris DJ, White RA. ERG phenotype of a dystrophin mutation in heterozygous female carriers of Duchenne muscular dystrophy. *J Med Genet*. 1999;36:316–322.
22. Barboni MT, Nagy BV, de Araujo Moura AL, et al. ON and OFF electroretinography and contrast sensitivity in Duchenne muscular dystrophy. *Invest Ophthalmol Vis Sci*. 2013;54:3195–3204.
23. McGreevy JW, Hakim CH, McIntosh MA, Duan D. Animal models of Duchenne muscular dystrophy: from basic mechanisms to gene therapy. *Dis Model Mech*. 2015;8:195–213.
24. Chamberlain JS, Farwell NJ, Chamberlain JR, Cox GA, Caskey CT. PCR analysis of dystrophin gene mutation and expression. *J Cell Biochem*. 1991;46:255–259.
25. Atorf J, Scholz M, Garreis F, Lehmann J, Brauer L, Kremers J. Functional protective effects of long-term memantine treatment in the DBA/2J mouse. *Doc Ophthalmol*. 2013;126:221–232.
26. Harazny J, Scholz M, Buder T, Lausen B, Kremers J. Electrophysiological deficits in the retina of the DBA/2J mouse. *Doc Ophthalmol*. 2009;119:181–197.
27. Saszik SM, Robson JG, Frishman LJ. The scotopic threshold response of the dark-adapted electroretinogram of the mouse. *J Physiol*. 2002;543:899–916.
28. Kremers J, Pangeni G, Tsaousis KT, McKeefry D, Murray IJ, Parry NR. Incremental and decremental L- and M-cone driven ERG responses: II. Sawtooth stimulation. *J Opt Soc Am A Opt Image Sci Vis*. 2014;31:A170–A178.
29. Schnapf JL, Kraft TW, Baylor DA. Spectral sensitivity of human cone photoreceptors. *Nature*. 1987;325:439–441.
30. Paupoo AA, Mahroo OA, Friedburg C, Lamb TD. Human cone photoreceptor responses measured by the electroretinogram a-wave during and after exposure to intense illumination. *J Physiol*. 2000;529(pt 2):469–482.
31. Akula JD, Lyubarsky AL, Naarendorp F. The sensitivity and spectral identity of the cones driving the b-wave of the rat electroretinogram. *Vis Neurosci*. 2003;20:109–117.
32. Kenkre JS, Moran NA, Lamb TD, Mahroo OA. Extremely rapid recovery of human cone circulating current at the extinction of bleaching exposures. *J Physiol*. 2005;567:95–112.
33. Lei B, Yao G, Zhang K, Hofeldt KJ, Chang B. Study of rod- and cone-driven oscillatory potentials in mice. *Invest Ophthalmol Vis Sci*. 2006;47:2732–2738.
34. Pangeni G, Lammer R, Tornow RP, Horn FK, Kremers J. On- and off-response ERGs elicited by sawtooth stimuli in normal subjects and glaucoma patients. *Doc Ophthalmol*. 2012;124:237–248.
35. Tsai TI, Atorf J, Neitz M, Neitz J, Kremers J. Rod- and cone-driven responses in mice expressing human L-cone pigment. *J Neurophysiol*. 2015;114:2230–2241.
36. Yang S, Luo X, Xiong G, So KF, Yang H, Xu Y. The electroretinogram of Mongolian gerbil (Meriones unguiculatus): comparison to mouse. *Neurosci Lett*. 2015;589:7–12.
37. Peachey NS, Goto Y, al-Ubaidi MR, Naash MI. Properties of the mouse cone-mediated electroretinogram during light adaptation. *Neurosci Lett*. 1993;162:9–11.
38. Chrysostomou V, Crowston JG. The photopic negative response of the mouse electroretinogram: reduction by acute elevation of intraocular pressure. *Invest Ophthalmol Vis Sci*. 2013;54:4691–4697.
39. Shirato S, Maeda H, Miura G, Frishman LJ. Postreceptoral contributions to the light adapted ERG of mice lacking b-waves. *Exp Eye Res*. 2008;86:914–928.
40. Kremers J, Scholl HPN. Rod-/L-cone and rod-/M-cone interactions in electroretinograms at different temporal frequencies. *Vis Neurosci*. 2001;18:339–351.
41. Weymouth AE, Vingrys AJ. Rodent electroretinography: methods for extraction and interpretation of rod and cone responses. *Prog Retin Eye Res*. 2008;27:1–44.
42. Sharma S, Ball SL, Peachey NS. Pharmacological studies of the mouse cone electroretinogram. *Vis Neurosci*. 2005;22:631–636.
43. Nagy BV, Barboni MT, Martins CM, da Costa MF, Kremers J, Ventura DF. Human flicker electroretinography using different temporal modulations at mesopic and photopic luminance levels. *Doc Ophthalmol*. 2014;129:129–138.
44. Jensen H, Warburg M, Sjo O, Schwartz M. Duchenne muscular dystrophy: negative electroretinograms and normal dark adaptation. Reappraisal of assignment of X linked incomplete congenital stationary night blindness. *J Med Genet*. 1995;32:348–351.
45. Pillers DA, Bulman DE, Weleber RG, et al. Dystrophin expression in the human retina is required for normal function as defined by electroretinography. *Nat Genet*. 1993;4:82–86.
46. Girlanda P, Quartarone A, Buceti R, et al. Extra-muscle involvement in dystrophinopathies: an electroretinography and evoked potential study. *J Neurol Sci*. 1997;146:127–132.
47. Dong CJ, Agey P, Hare WA. Origins of the electroretinogram oscillatory potentials in the rabbit retina. *Vis Neurosci*. 2004;21:533–543.
48. Wachtmeister L. Oscillatory potentials in the retina: what do they reveal. *Prog Retin Eye Res*. 1998;17:485–521.
49. Algevere P, Westbeck S. Human ERG in response to double flashes of light during the course of dark adaptation: a Fourier analysis of the oscillatory potentials. *Vis Res*. 1972;12:195–214.
50. Werblin FS. Regenerative amacrine cell depolarization and formation of on-off ganglion cell response. *J Physiol*. 1977;264:767–785.
51. Granit R. The components of the retinal action potential in mammals and their relation to the discharge in the optic nerve. *J Physiol*. 1933;77:207–239.
52. Peachey NS, Sturgill-Short GM. Response properties of slow PIII in the Large (vls) mutant. *Doc Ophthalmol*. 2012;125:203–209.

Investigative Ophthalmology & Visual Science

53. Kofuji P, Ceelen P, Zahs KR, Surbeck LW, Lester HA, Newman EA. Genetic inactivation of an inwardly rectifying potassium channel (Kir4.1 subunit) in mice: phenotypic impact in retina. *J Neurosci*. 2000;20:5733–5740.
54. Pascual SI, Molano J, Pacual-Castroviejo I. Electroretinogram in Duchenne/Becker muscular dystrophy. *Pediatr Neurol*. 1998; 18:315–320.
55. Nguyen CT, Vingrys AJ, Wong VH, Bui BV. Identifying cell class specific losses from serially generated electroretinogram components. *BioMed Res Int*. 2013;2013:796362.
56. Connors NC, Kofuji P. Dystrophin Dp71 is critical for the clustered localization of potassium channels in retinal glial cells. *J Neurosc*. 2002;22:4321–4327.
57. Bringmann A, Pannicke T, Grosche J, et al. Müller cells in the healthy and diseased retina. *Prog Retin Eye Res*. 2006;25:397–424.
58. Raz-Prag D, Grimes WN, Fariss RN, et al. Probing potassium channel function in vivo by intracellular delivery of antibodies in a rat model of retinal neurodegeneration. *Proc Natl Acad Sci U S A*. 2010;107:12710–12715.
59. Holder GE. Electrophysiological assessment of optic nerve disease. *Eye (Lond)*. 2004;18:1133–1143.
60. Fritsch D, Muntoni F, Grunewald S, Sowden J, Thompson D. Visual evoked potentials in ON-pathway disorders. Paper presented at: 53rd Symposium of International Society for Clinical Electrophysiology of Vision (ISCEV), June 23–25, 2015, Ljubljana, Slovenia.
61. De Becker I, Riddell DC, Dooley JM, Tremblay F. Correlation between electroretinogram findings and molecular analysis in the duchenne muscular-dystrophy phenotype. *Br J Ophthalmol*. 1994;78:719–722.
62. Wassle H. Parallel processing in the mammalian retina. *Nat Rev Neurosci*. 2004;5:747–757.
63. Kremers J. Signal pathways in the electroretinogram. In: Belušič G, ed. *Electroretinograms*. Rijeka: InTech; 2011:55–78.
64. Cleland BG, Levick WR, Sanderson KJ. Properties of sustained and transient ganglion cells in the cat retina. *J Physiol*. 1973; 228:649–680.
65. Nirenberg S, Meister M. The light response of retinal ganglion cells is truncated by a displaced amacrine circuit. *Neuron*. 1997;18:637–650.
66. Awatramani GB, Slaughter MM. Origin of transient and sustained responses in ganglion cells of the retina. *J Neurosci*. 2000;20:7087–7095.
67. Haenggi T, Fritschy JM. Role of dystrophin and utrophin for assembly and function of the dystrophin glycoprotein complex in non-muscle tissue. *Cell Mol Life Sci*. 2006;63: 1614–1631.
68. Selsby JT, Ross JW, Nonneman D, Hollinger K. Porcine models of muscular dystrophy. *ILAR J*. 2015;56:116–126.

Investigative Ophthalmology & Visual Science